nature protocols

PROTOCOL

https://doi.org/10.1038/s41596-018-0031-8

Mapping heterogeneity of cellular mechanics by multi-harmonic atomic force microscopy

Yuri M. Efremov[1,2,7], Alexander X. Cartagena-Rivera[3,7], Ahmad I. M. Athamneh[2,4], Daniel M. Suter[2,4,5,6] and Arvind Raman[1,2*]

The goal of mechanobiology is to understand the links between changes in the physical properties of living cells and normal physiology and disease. This requires mechanical measurements that have appropriate spatial and temporal resolution within a single cell. Conventional atomic force microscopy (AFM) methods that acquire force curves pointwise are used to map the heterogeneous mechanical properties of cells. However, the resulting map acquisition time is much longer than that required to study many dynamic cellular processes. Dynamic AFM (dAFM) methods using resonant microcantilevers are compatible with higher-speed, high-resolution scanning; however, they do not directly acquire force curves and they require the conversion of a limited number of instrument observables to local mechanical property maps. We have recently developed a technique that allows commercial AFM systems equipped with direct cantilever excitation to quantitatively map the viscoelastic properties of live cells. The properties can be obtained at several widely spaced frequencies with nanometer-range spatial resolution and with fast image acquisition times (tens of seconds). Here, we describe detailed procedures for quantitative mapping, including sample preparation, AFM calibration, and data analysis. The protocol can be applied to different biological samples, including cells and viruses. The transition from dAFM imaging to quantitative mapping should be easily achievable for experienced AFM users, who will be able to set up the protocol in <30 min.

Introduction

The local mechanical properties of living cells, such as viscoelasticity and adhesion, are far from homogeneous across the cell. In fact, heterogeneities in these nanomechanical properties play important roles in a majority of cellular processes, including morphogenesis[1], mechanotransduction[2], motility[3–6], metastasis[7–9], and response to drugs[10–12], and can act as efficient disease markers[13–15]. Changes in mechanical properties are increasingly recognized for their organizational role in cells, often occurring only in localized regions and over short periods of time, leading to spatiotemporal mechanical heterogeneity in the cell. Examples include spatially localized cell–cell and cell–extracellular matrix interactions[16,17], asymmetric force generation during cell motility[18], and the nonuniform reinforcement of the cell's rigidity by the cytoskeleton[19]. Consequently, many interesting mechanobiological questions address very local and highly dynamic aspects of the cell. Thus, there is a growing interest in mapping mechanical heterogeneities within living cells with high spatiotemporal resolution. A large variety of methods have been introduced for measuring cellular mechanical properties, including micropipette aspiration[20], stretching or compression between two microplates[21,22], optical tweezers[23,24], and magnetic twisting cytometry[25,26]. However, AFM remains one of the most popular and most suitable methods for probing the properties of soft samples at the nanometer scale[10,27–31]. Various AFM techniques have been developed for this purpose, including quasi-static ones that measure force during the indentation of the sample[32–36] and dynamic ones (dAFM)[37–39] that either vibrate the cantilever or the sample and measure variations in the response of the cantilever that are due to interaction with the sample.

Achieving high-speed mapping of nanomechanical properties of whole live eukaryotic cells (elastic modulus <100 kPa), over large areas (~50 × 50 μm^2), and with a wide range of topographies (cell height ~1–10 μm) has been a long-standing challenge in dAFM[40,41]. This is due to the softness of live

[1]School of Mechanical Engineering, Purdue University, West Lafayette, IN, USA. [2]Birck Nanotechnology Center, Purdue University, West Lafayette, IN, USA. [3]Laboratory of Cellular Biology, Section on Auditory Mechanics, National Institute on Deafness and Other Communication Disorders, Bethesda, MD, USA. [4]Department of Biological Sciences, Purdue University, West Lafayette, IN, USA. [5]Bindley Bioscience Center, Purdue University, West Lafayette, IN, USA. [6]Purdue Institute for Integrative Neuroscience, Purdue University, West Lafayette, IN, USA. [7]These authors contributed equally: Yuri M. Efremov, Alexander X. Cartagena-Rivera. *e-mail: raman@purdue.edu

eukaryotic cells, which reduces the sensitivity of dAFM observables such as amplitude and phase, and because of the large height variations of live cells, which require a high *z*-piezo positioning range. Moreover, problems related to hydrodynamic effects (fluid-borne forest of peaks in the excitation spectrum and squeeze-film damping effects in the near vicinity of the sample surface) must be solved by direct-excitation techniques and a specific design of the cantilevers[28,42].

Here, we present details of an advanced dAFM method that we recently developed to quantitatively map the nanomechanical properties of soft biological samples in a liquid environment[28,37,43,44] (Fig. 1). This multi-harmonic AFM biomechanical cell assay method is completely compatible with commercial AFM systems equipped with a direct-excitation setup.

Development of the approach

Our method is based on the amplitude-modulated mode of dAFM (AM-AFM), which is also known as the tapping mode. In this approach, the sharp nanoscale tip of the cantilever interacts with the sample while its *z* position is adjusted to regulate the oscillation amplitude while scanning over the surface. In a liquid environment, which is physiological for most biological samples, direct excitation of the cantilever (e.g., magnetic excitation; see also 'Experimental design') is required to obtain well-behaved transfer functions that relate the oscillation observables (amplitudes and phases) and the calibrated cantilever characteristics (spring constant and the quality factor (Q); Fig. 1). On the basis of the mechanical properties of the sample, two main situations are possible when the cantilever tip interacts with the sample. In the first, when the sample is relatively stiff (modulus in the ~10-MPa range or larger, such as is the case for viruses and bacteria), the tip only intermittently taps on the sample, introducing short- and long-range tip–sample interaction forces (F_{ts}). The nonlinearity of these combined electrostatic, elastic, and hydration forces, together with the low Q factors in liquids for low-stiffness cantilevers, leads to anharmonics in the cantilever vibration spectrum of the excitation frequency. On harder samples, many anharmonics can be generated[38,39,45,46]; however, on moderately stiff to soft samples (modulus ~10 MPa or smaller), only a small set of anharmonics are usually observed, especially at $0\omega_{dr}$,$1\omega_{dr}$, and $2\omega_{dr}$[37,44], where ω_{dr} is the excitation frequency. Thus, the amplitudes (A_0, A_1, and A_2) and phases (ϕ_1 and ϕ_2) at these frequencies boost the available independent observables for material contrast[37,44]. We have developed a theory that links these multi-harmonic observables to the local mechanical properties of the sample, which are stiffness k_{sample} ($N \cdot m^{-1}$) and damping c_{sample} ($N \cdot s \cdot m^{-1}$), as described below. Together, they represent the parameters of an equivalent Kelvin–Voigt element and can be regarded as the local viscoelastic properties. However, we have shown previously[37] that a different situation arises on very soft samples such as living cells and hydrogels (modulus <~1 MPa). At the imaging set point, the tip is not intermittently 'tapping' the cell as it does on harder surfaces, but rather the tip 'permanently' interacts with the cell over its entire oscillation cycle while maintaining a large net average indentation[43]. The tip oscillation amplitude is small as compared with the average indentation, and this allows the Taylor series representation for use of well-validated elastic contact mechanics models such as Hertz's[47] or Sneddon's[48], or models with bottom-effect correction[49,50]. This provides high-resolution nanomechanical maps showing local heterogeneity in mechanical properties such as the complex elastic modulus of the viscoelastic sample ($E^* = E^{storage} + iE^{loss}$) (Fig. 1). The real part of it, storage modulus $E^{storage}$, is a measure of a material's stored elastic energy portion, and the imaginary part, loss modulus E^{loss}, measures the material's energy-dissipated (viscous) portion.

Overview of the procedure

The purpose of this protocol is to obtain nanomechanical property maps of whole live eukaryotic cells, bacteria, viruses, or other biological samples (e.g., extracellular matrix gels and tissue sections) with high temporal and spatial resolution. Here, we demonstrate the setup for murine fibroblasts and neuronal growth cones. The method allows the study of time-varying heterogeneous physical properties of live cells during dynamic processes over large areas[51]. The procedure consists of three main stages (Fig. 1). In the first stage, we provide step-by-step instructions for how to prepare cell samples (Steps 1 and 2), set up the AFM and optical microscope (Steps 3–8), and perform calibrations (Steps 9 and 10). In the second stage, we describe how to perform a multi-harmonic AFM-imaging procedure (Steps 11–17). Harmonic observables (amplitudesA_0, A_1, and A_2 and phases ϕ_1 and ϕ_2) are recorded simultaneously with topography during scanning of the sample with a directly excited cantilever. The scanning is performed with the feedback applied on the deflection signal. In the third stage, we provide guidance for data processing (Steps 18 and 19). First, the

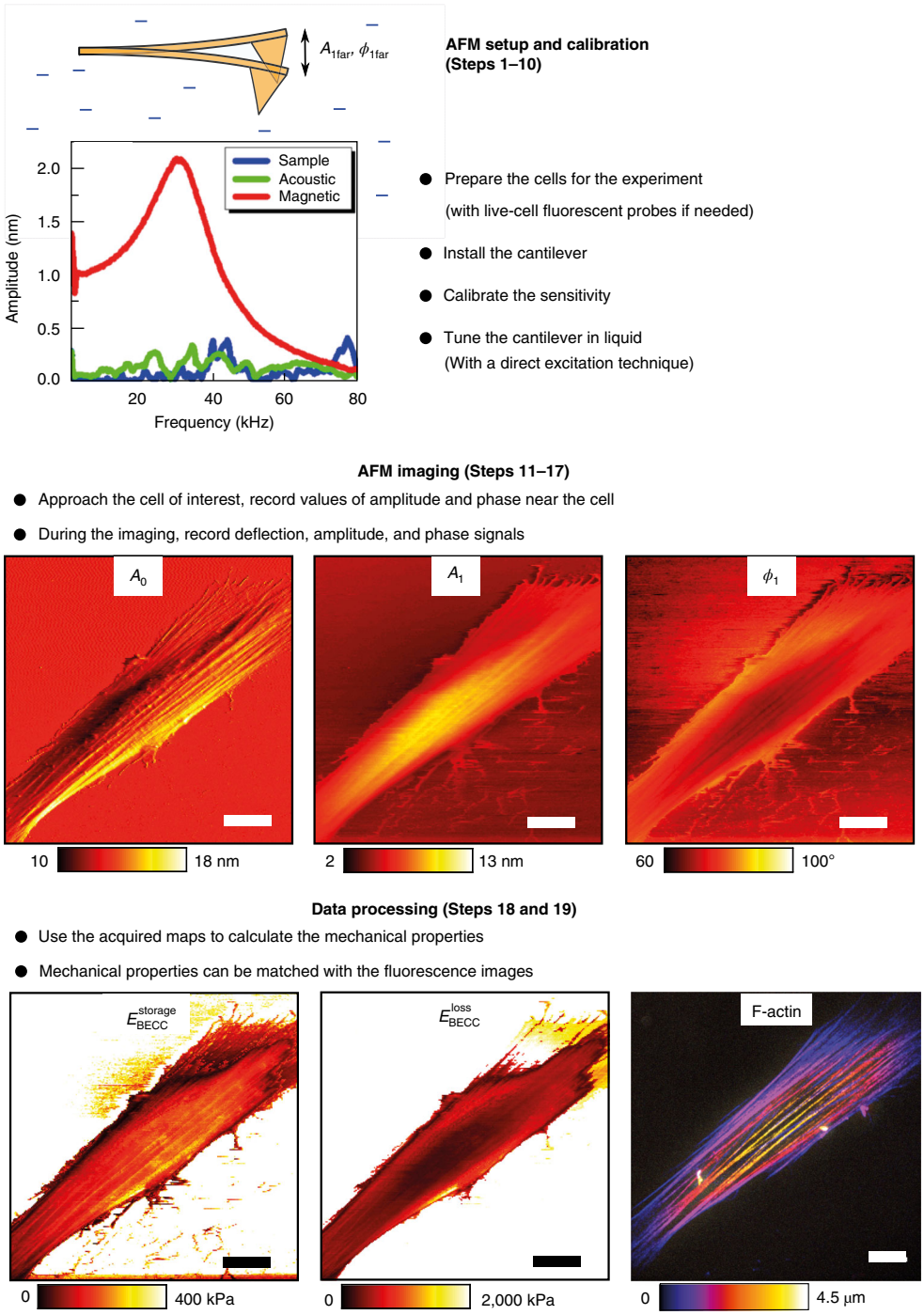

Fig. 1 | Overview of the protocol. In Steps 1 and 2, the sample is prepared, followed by setup of the AFM (Steps 3–8) and calibration of the AFM setup in Steps 9 and 10. A direct cantilever excitation method is used (iDrive) that retains the transfer function of a single harmonic oscillator in liquid, whereas indirect techniques (acoustic and sample excitation) do not[28]. In Steps 11–17, AFM imaging is performed and maps of the multi-harmonic observables (amplitudes A_0, A_1, and phase ϕ_1) are acquired. For the AFM scanning, the mean deflection is used as feedback signal. In Steps 18 and 19, the mechanical properties (storage and loss moduli with the bottom-effect cone correction (BECC)) are calculated from the acquired observables using the theory described in the Introduction. Heterogeneities in local mechanical properties can be matched with the actin cytoskeleton structure in the studied cell (right, spinning-disk confocal microscopy, color-coded *z* projections of the SiR-actin staining). Scale bars, 10 µm.

observables are converted into harmonic tip-surface conservative and dissipative forces. Last, direct analytical equations or nonlinear least-squares algorithms are used to find material properties from the observables.

Extracting local cellular mechanical properties

Detailed descriptions of methods for data analysis are available[28,37,43,44]. The theory behind this is presented in the Supplementary Theory and described briefly below. Assuming that the directly excited cantilever driving frequency is near the natural frequency of the fundamental flexural mode, the steady-state motion of the tip interacting with the sample surface is composed of harmonics so that the tip displacement is

$$q(t) = A_0 + A_1 \sin(\omega_{dr} t - \phi_1) + A_2 \sin(2\omega_{dr} t - \phi_2) + O(\varepsilon), \quad (1)$$

where A_0 is the zeroth harmonic amplitude (cantilever mean deflection), ω_{dr} is the cantilever driving frequency, A_1 is the first harmonic amplitude (the traditional feedback signal for AM-AFM), ϕ_1 is the first harmonic phase, A_2 is the second harmonic amplitude, and ϕ_2 is the second harmonic phase. In liquids, the zeroth, first, and second harmonics are dominant harmonics that describe the tip motion and can be easily recorded simultaneously during experiments.

Because the tip motion is periodic, the tip–sample interaction force must also be periodic. This leads to the following Fourier expansion of the tip–sample interaction force in terms of conservative and dissipative components:

$$F_{ts} = F^0_{ts,CONS} + \sum_{n=1}^{\infty} F^n_{ts,DISS} \cos(n\theta) + \sum_{n=1}^{\infty} F^n_{ts,CONS} \sin(n\theta), \quad (2)$$

where F_{ts} is the tip–sample interaction force, $F_{ts,CONS}$ is the force conservative component, $F_{ts,DISS}$ is the force dissipative component, and $\theta = \omega_{dr} t - \phi$.

The quantitative measurement of the zeroth and first harmonic of interaction forces is sufficient to determine the relevant mechanical properties of living cells, the viscoelastic storage, and loss modulus. We used the bottom-effect cone correction (BECC) model[50] to derive exact close-form analytical formulas that relate the measured tip–sample force harmonics to the mechanical properties $E^{storage}$ and E^{loss}.

$$\begin{aligned} F^0_{ts,CONS} &= \frac{8E^{storage}_{BECC} \tan(\alpha)\delta_0^2}{3\pi}\left(1 + a_1\frac{\delta_0}{h} + a_2\frac{\delta_0^2}{h^2}\right), \\ F^1_{ts,CONS} &= \frac{-8E^{storage}_{BECC} \tan(\alpha)\delta_0}{3\pi}\left(2 + 3a_1\frac{\delta_0}{h} + 4a_2\frac{\delta_0^2}{h^2}\right)A_1, \\ F^1_{ts,DISS} &= \frac{-8E^{loss}_{BECC} \tan(\alpha)\delta_0}{3\pi}\left(2 + 3a_1\frac{\delta_0}{h} + 4a_2\frac{\delta_0^2}{h^2}\right)A_1. \end{aligned} \quad (3)$$

where $E^{storage}_{BECC}$ is the elastic storage modulus using the BECC model, E^{loss}_{BECC} is the viscous loss modulus using the BECC model, $\delta_0$is the sample mean indentation, α is the AFM tip half-opening angle, h is the finite thickness of the sample, a_1 and a_2 are the coefficients from the multiplicative analytical correction[50], and the Poisson's ratio is assumed to be 0.5 for soft samples such as living cells. This method, using the BECC model, will lead to better estimates of mechanical properties on thinner parts of the biological sample. Using these expressions, a nonlinear least-squared fit is performed pointwise on the force harmonic maps to find those values of the mechanical properties that best fit the force harmonics. See the Supplementary Theory for a detailed description of the theory. Note that most commonly used contact mechanics models in AFM can be combined with this method to measure material properties.

Comparison with other AFM methods

The method presented here for extracting local mechanical properties is different from conventional methods that acquire force–distance AFM (F–z) curves by moving pointwise over the sample. In the case of F–z curves, the entire curve is fitted to a continuous mechanics model starting from the first point of contact, whereas in this protocol, a small subset of dAFM multi-harmonic observables is tracked to map the local effective force gradients at a specific mean indentation value that changes from point to point on the image. Second, the conventional F–z curves are generally analyzed in a purely elastic context, and only recently have some attempts been made to acquire viscoelastic properties by this technique[32,35,36]. The effective properties obtained using the method presented herein correspond to viscoelastic properties measured at much higher frequencies (acoustic) than conventional F–z curves. Because the viscoelastic properties of biomaterials are strongly frequency dependent, the values extracted using the multi-harmonic method are expected to be different from those of the quasi-static method[43]. Moreover, the imaging throughput of the described method in

mapping local mechanical properties of cells represents ~10×–1,000× improvement in imaging throughput as compared with the standard force–volume method.

New methods have been introduced to improve the spatiotemporal resolution for the pointwise acquisition of force curves over the sample, such as the quantitative imaging mode of JPK Instruments[52] and the peak force tapping method of Bruker AFM systems[53–55]. These new methods have substantially improved the speeds for mapping cellular mechanical properties of biological samples as compared with those for the conventional quasi-static force–volume method. However, the acquisition times for a high-resolution material property map of an entire eukaryotic cell remain on the order of a minute, which is slower than many cellular dynamic processes of interest. In addition, the mentioned alternative methods are currently unable to determine the constitutive viscosity of cells.

Applications and limitations of the protocol

We have applied this protocol to different types of samples, including adherent animal cells[37,43,51], human red blood cells[37], bacterial cells[37], and viruses[44]. The measurable elasticity range compares with the measurable range for using traditional force–distance curve spectroscopy. Both soft cancerous cells (kiloPascals) and stiff mature virions (megaPascals) were successfully studied. The range can be further expanded by using softer or stiffer cantilevers whenever needed, as the force sensitivity depends on the cantilever spring constant. The available frequency range also depends on the selected cantilever, more specifically on its resonance frequency in liquid. Both lower and higher frequencies can be used; the effective range is determined by the noise level in the liquid and the efficiency of the excitation technique (it generally ranges from hundreds of Hertzes to hundreds of kiloHertzes).

This approach shares the common limitations of any AFM technique: (i) the sample should adhere to a surface well enough to withstand the mapping process, (ii) it should not adhere too strongly to the cantilever tip, and (iii) the surface should be accessible for the analysis. Furthermore, accessible scan areas and rates are limited by the construction of piezoscanners. There is still room for improvement here, including the development of fast scanners with short response times[56]. Last, direct-excitation techniques are not available on all commercial AFM systems and usually require the specific design of the cantilevers (Experimental design).

We believe that the developed protocol may find applications in the studies of cellular mechanosensation, mechanoresponse, and motility, especially when high spatiotemporal resolution is required. There is an emerging need for a better understanding of the fast time-varying mechanical properties of living cells, as there is a close interplay between chemical and mechanical signaling[57]. This is particularly critical for increasing our knowledge of the underlying mechanisms of cell proliferation, differentiation, and migration in normal and disease states. Cells respond not only to molecular and topographical cues but also to mechanical cues from the environment. To better comprehend how cells respond to all these cues, we must analyze both intracellular signal transduction with high spatiotemporal resolution and the subcellular mechanical properties. In summary, mapping mechanical properties of migrating cells will advance our understanding of not only normal organism development and function but also of disease states such as neuronal degeneration, inflammation, and tumor progression (see Anticipated results).

Experimental design

Direct-excitation techniques

Many direct- and indirect-excitation techniques are commonly used for dAFM in liquids[58–62]. However, for extracting quantitative information, direct excitation is required, as it leads to well-defined microcantilever dynamics in liquids (Fig. 1). The most frequently used direct-excitation methods are magnetic[58,59] and photothermal[60,61] actuation. The acoustic mode is the most widely used indirect-excitation method; in this method, vibration of a piezoelectric transducer attached to the cantilever holder excites the microcantilever[58]. However, this excitation method drives not only the cantilever but also the chip, holder, and surrounding liquid[58]. This generates an effect called 'forest of peaks'[28,58,63] that masks out the real microcantilever vibration response. A second arising effect is that fluid-borne excitation has a major influence on cantilever dynamics, even if the forest-of-peaks effect is resolved[64].

Photothermal excitation uses a high-powered laser that is focused on the back of the cantilever; the power of this laser is modulated, causing a heat gradient to excite AFM microcantilevers[60,61]. However, its photothermal efficiency is low and requires high laser power to mechanically actuate the cantilever for a few nanometers, resulting in local heat that can potentially damage sensitive samples

and accelerate liquid evaporation[60]. For direct 'magnetic' excitation, two setups exist: (i) magnetic, which consists of a paramagnetic coating on the microcantilever backbone that will be excited by a solenoid such that applying an alternating current to it generates a magnetic field that interacts and excites the coated microcantilever[65–67]; and (ii) Lorentz force excitation, which is a technology that consists of a triangular gold-coated V-shaped cantilever (iDrive mode for Asylum Research AFMs)[59]. An alternating current is applied to the cantilever, generating an electric field that will interact with a magnetic field generated by a permanent magnet. This technique avoids the use of magnetic materials on the cantilever and the requirement for oscillating magnetic fields. Directly excited cantilevers have a well-defined transfer function with the Lorentz/photothermal force being the only source of excitation, avoiding interference from fluid-borne excitation that arises when either the cantilever or the sample is excited using piezoelectric transducers[58]. The limitation of the iDrive technique is the requirement for both a specialized cantilever holder and specialized cantilevers (see the Selection of the cantilever section below).

The developed method is completely compatible with the described direct-excitation setups, both commercially available (iDrive and blueDrive for Asylum Research AFMs, and the MAC Mode for Keysight Technologies AFMs[67]) and custom-made[65,66]. Here, we will describe the protocol using only the Lorentz force excitation technique (iDrive) because of its ease of operation, quantitative robustness, and protocol conciseness. Only slight modifications in the protocol will be required to use another direct-excitation technique. Specifically, in Step 9 'Performing calibrations', the AFM manufacturer's guidelines related to a specific direct-excitation setup should be followed.

Selection of the cantilever

The cantilever should be compatible with the direct-excitation technique used. For example, BL-TR400PB (Asylum Research) cantilevers are specially designed for the iDrive mode. A wider spectrum of cantilevers is compatible with the photothermal excitation technique[60]. Important aspects when selecting a cantilever for quantitative nanomechanical measurements also include stiffness, tip height, beam area (hydrodynamic shape), shape of the tip, and the cantilever itself. Soft cantilevers are generally preferable for studying soft samples (<0.1 $nN \cdot nm^{-1}$). Longer tips (~10 μm) are more suitable for tall samples such as cells because they prevent interactions between the sides of a tip, the cantilever beam, and the cell surface[68]. In addition, longer tips reduce the hydrodynamic damping due to squeeze-film effects that develop between the oscillating plane of the cantilever and a rigid surface[42]. For the same reason, cantilevers with a smaller surface are preferable. Very sharp cantilever tips should be avoided, as they can damage living cells[69]. High resolution was obtained in living cells with relatively dull cantilever tips (65-nm radius), emphasizing the role of the low imaging forces over the tip sharpness[54].

Boosting the scanning speed by applying feedback to the deflection signal

The appropriate choice of feedback channel can lead to substantial improvement of the scanning speed when using dAFM to scan soft samples such as living cells. As we showed previously[28], the sensitivity of the cantilever mean deflection (dA_0/dz) is several times larger than the sensitivity of the first harmonic amplitude (dA_1/dz; the traditional feedback channel) for living cells, especially in the nuclear region (~12 times) (Fig. 2). The low sensitivity of A_1 originates from the small repulsive-force gradients on a live cell and the low quality factor of the cantilever in liquid. A stronger gradient (dA_0/dz) allows use of the higher feedback gains and enables faster tracking of the cell topography. Overall, use of the mean deflection feedback while imaging live cells in culture medium with resonant cantilevers allows a considerable increase (~20×) in scanning speed for nanomechanical mapping of living cells as compared with traditional amplitude feedback. The cantilever remains in permanent contact with the cell during scanning, and the theory linking A_0, A_1, and ϕ_1 with local nanomechanical properties remains applicable.

Viscoelastic property mapping using two widely spaced frequencies

The method described here also allows for viscoelastic property mapping at widely spaced frequencies by simultaneously exciting the cantilever in the fundamental and second flexural eigenmode. Multimodal excitation such as bimodal[70,71] or trimodal[72] is able to boost the number of compositional contrast channels and has been demonstrated for fast scanning on live cells[28]. By comparison of mechanical properties at different frequencies, conclusions about the viscoelastic behavior of the sample can be made (Fig. 3). In the case of eukaryotic cells, an increase in the cell stiffness and damping with frequency is observed with this technique[28] and other techniques[73,74]. The

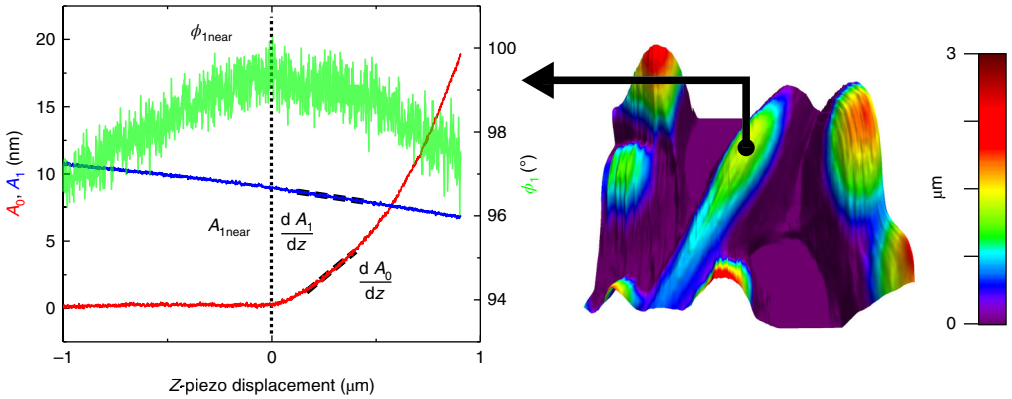

Fig. 2 | Typical dynamic approach curve obtained in the central region of a fibroblast cell (nuclear area) with a Lorentz excited cantilever. The behavior of the multi-harmonic amplitudes and phase (A_0, A_1, and ϕ_1) as the cantilever moves toward and interacts with the cell. Before the contact (z =0), A_1 decreases and ϕ_1 increases as a result of the near-surface squeeze-film hydrodynamic effect, reaching values of A_{1near} and ϕ_{1near}. After the contact, both decrease, whereas A_0 increases. The gradient dA_0/dz is much larger than dA_1/dz, making it a better choice for the feedback channel.

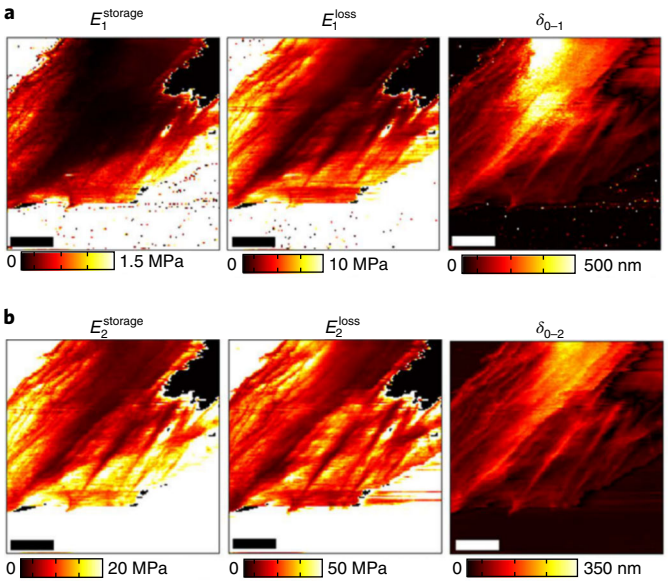

Fig. 3 | Bimodal AFM on a rat fibroblast. a, Maps of local elastic storage modulus, viscous loss modulus, and mean indentation extracted from the measured first-mode data (f_1=7.06 kHz). **b**, The same maps extracted from the measured second-mode data ($f_2 = 61.33$ kHz) using the theory described in the Introduction and in the Supplementary Theory. Scale bars, 6 μm; acquisition time of maps = 2 min 30 s; 256 × 256 pixels. Adapted from Cartagena-Rivera et al.[28] (https://www.nature.com/articles/srep11692; original material licensed under a Creative Commons Attribution License 4.0).

high–frequency viscoelastic measurements of live cells are scarce but potentially relevant[75], as existing power-law-based microrheological models[76] of live cells are generally confirmed only for small frequencies (<1 kHz)[74]. The dynamics of individual cytoskeleton filaments are expected to emerge at short time scales; thus, high-frequency maps can help assess the morphological and dynamical state of the cytoskeleton[28,37]. Overall, simultaneous nanomechanical mapping at several frequencies can help to better distinguish cell type and state.

Combining multi-harmonic AFM with fluorescence techniques

A combined AFM-optical microscope provides large benefits for characterizing biological samples over the AFM-only setup[52,77–86]. First, trans-illumination or fluorescence imaging can be used to direct the cantilever to the area of interest. Second, the ability of optical techniques to image

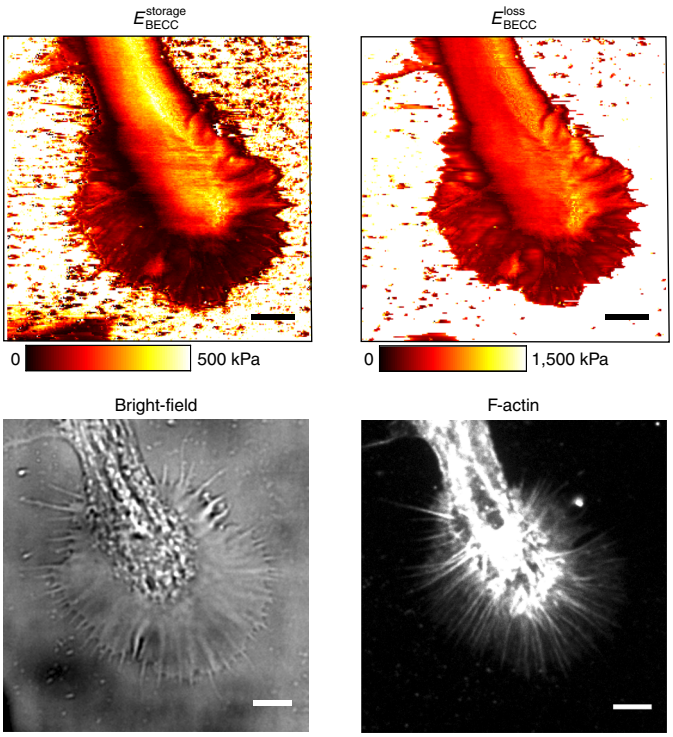

Fig. 4 | Comparison of AFM nanomechanical with fluorescence data in a growth cone developed by an *Aplysia* bag cell neuron. Maps of the mechanical properties (storage and loss moduli, and bottom-effect cone correction model), bright-field image, and fluorescent actin image after SiR-actin labeling. Filopodia actin fibers correspond to stiffer regions on the maps, in agreement with the previous study[96]. Scale bars, 5 μm; acquisition time of maps = 5 min; 256 × 256 pixels.

within the depth of a sample using label-conjugated (e.g., fluorescent) markers allows researchers to identify specific structures or molecules inside or on the surface of a sample. Coupled with AFM data for high-resolution nanomechanical properties, a more complete understanding of the structure–function relationships of living cells can be elucidated (Figs. 1 and 4). The two datasets can be directly overlaid, compared, and correlated[85]. Moreover, fluorescent techniques can be used to stimulate the cells of interest and observe the changes in mechanical properties by AFM, and vice versa.

We use a custom-built integrated AFM/SDC (spinning-disk confocal) system for simultaneous mechanical mapping and fluorescence imaging. SDC microscopes are well suited to imaging of living cells because of their high image acquisition speed and low laser intensities[87]. Live-cell imaging requires special fluorescent probes, some of which have been shown to alter properties of the studied protein/molecule and overall cell behavior[88,89]. Therefore, selection of the appropriate fluorescent probe and its concentration should be performed with caution, and control experiments without the probe are desirable. Furthermore, one could take advantage of super-resolution fluorescence techniques, but usually they are associated with slower image acquisition speeds.

Materials

Biological materials

- NIH 3T3 fibroblasts (ATCC, cat. no. CRL-1658) **! CAUTION** Follow all relevant ethics guidelines and laws when working with human cells or tissues. The cell lines used should be regularly checked to ensure that they are authentic and are not infected with mycoplasma.
- Primary *Aplysia* bag cell neuron cultures. The protocol for isolation of *Aplysia* bag cell neurons is described in refs [90,91].

Reagents

- DMEM cell culture medium (low glucose, GlutaMAX, pyruvate; Gibco, cat. no. 10567014)
- FBS (Gibco, cat. no. 10437-077)

- CO_2-independent cell culture medium (Gibco, cat. no. 18045088)
- PBS without Ca^{2+} and Mg^{2+} (Gibco, cat. no. 10010023)
- 100× antibiotic–antimycotic solution (Gibco, cat. no. 15240062)
- Fibronectin solution (1 mg/mL; Sigma, cat. no. F1141)
- Poly-L-lysine solution (0.01% (wt/vol); Sigma, cat. no. P4707)
- HEPES solution (1 M, pH 7.0–7.6; Sigma, cat. no. H0887)
- Triton X-100 (Sigma, cat. no. T8787)
- L15-ASW medium (a protocol for the preparation is described in refs [90,91])
- (Optional) Fluorescent markers for the cell components that will be imaged with the fluorescence microscopy. We used the SiR-actin dye (Cytoskeleton) for visualization of actin cytoskeleton[92].

Equipment

- AFM system (Oxford Instruments, model no. Asylum MFP-3D Bio) ▲ **CRITICAL** Alternative AFM systems, such as one for biological samples with a Petri dish holder, heater, and a direct cantilever excitation setup, can be used.
- Inverted optical microscope (Olympus, model no. IX-71)
- Petri dish holder and heater with environmental controller (Asylum Research)
- Glass-bottom cell culture dishes (50 mm, FluoroDish; World Precision Instruments, cat. no. FD5040-100)
- Vibration table (Kynetic Systems)
- Acoustic isolation enclosure (Oxford Instruments)
- Objectives (10×, 40×, and 100×; Olympus)
- (Optional) Phase-contrast, differential interference contrast (DIC), fluorescence, or confocal setup for the optical microscope. We used a spinning-disk confocal microscope (Andor Technology, Revolution XD model) for the acquisition of fluorescence images.
- Camera (cooled charge-coupled camera; PhotoMetrics, CoolSnap MYO model)
- iDrive module for Lorentz-force-induced direct excitation of cantilevers (Asylum Research)
- Soft cantilevers with a nominal spring constant of 0.09 N/m, a nominal tip radius of 42 nm (±12 nm), and half-opening angle $\alpha = 35°$ (Olympus/Asylum Research, model no. BL-TR400PB) ▲ **CRITICAL** Cantilever choice is a critical parameter in these experiments. Cantilevers should be compatible with direct-excitation technique (iDrive was used here) and suitable for soft samples.

Software

- MATLAB v.R2014B or higher (MathWorks, http://www.mathworks.com)
- MATLAB scripts for data processing (Supplementary Data)

Reagent setup

Complete cell culture medium

Complete cell culture medium is DMEM supplemented with 10% (vol/vol) FBS and 1% (vol/vol) antibiotic–antimycotic solution. Store the complete cell medium at 4 °C for up to 2 weeks.

Fibronectin-coated cell culture dishes

Dilute the stock 1 mg/mL fibronectin solution with sterile PBS to create a 30 μg/mL fibronectin working solution. Store the working solution at 4 °C for up to 6 months. Coat the 50-mm glass-bottom cell culture dishes by incubating them for 30 min with 0.5-mL of fibronectin working solution. Aspirate the working solution and wash the dish three times with sterile PBS. Store the modified dishes at 4 °C for up to 2 weeks.

Poly-L-lysine–coated cell culture dishes

Coat the 50-mm glass-bottom cell culture dishes by incubating them for 5 min with 1 mL of 0.01% (wt/vol) poly-L-lysine solution. Aspirate the poly-L-lysine solution and wash the dish three times with sterile PBS. Store the modified dishes at 4 °C for up to 2 weeks.

Medium for AFM experiments

HEPES buffer can be added to the cell medium to create a CO_2-independent medium. Add 20 μL of 1 M HEPES solution per 1 mL of complete cell culture medium. Alternatively, a commercially

available product could be used. Supplement the CO_2-independent medium with 1% (vol/vol) antibiotic–antimycotic solution. Store the medium solution at 4 °C for up to 2 weeks.

Cleaning solution for cantilevers
Dilute Triton X-100 with PBS to create a 0.5% (vol/vol) working solution. Store the working solution at 4 °C for up to 1 month.

Procedure

Preparation of cells for AFM ● Timing 15 min, followed by 1–2 d of culture

1. To prepare cells for AFM experiments, seed the NIH 3T3 cells in complete cell culture medium onto fibronectin-coated 50-mm glass-bottom cell culture dishes (Reagent setup). Let the cells grow for an additional period of 1−2 d to a final confluency of ~60–70%.
   ▲ CRITICAL STEP We have also used our approach for mapping viscoelastic properties in different cell types, such as primary *Aplysia* bag cell neurons (Anticipated results). Primary *Aplysia* bag cell neurons should be grown in L15-ASW medium on poly-L-lysine-coated 50-mm glass-bottom cell culture dishes (Reagent setup). Incubate the cells for 1–2 d at 14 °C until well-developed growth cones can be seen.
   ▲ CRITICAL STEP Do not grow cells to >70% confluency.
2. (Optional) To label F-actin in live cells, incubate the cells with 200 nM SiR-actin for 12 h on the day after cell plating.

Setup of the AFM and optical microscope ● Timing 15 min

3. Turn on the AFM, associated instruments, and software.
4. Take the glass-bottom Petri dish containing the NIH 3T3 cells and replace the cell culture medium with the CO_2-independent medium for AFM (Reagent setup). Place the dish in the Petri dish holder of the AFM setup and set the environment control system to 37 °C.
   ▲ CRITICAL STEP Experiments on *Aplysia* bag cell neurons should be performed at room temperature (18–25 °C) in L15-ASW medium.
5. Mount a BL-TR-400PB cantilever into the cantilever holder.
6. Insert the cantilever holder into the AFM head and position the head on the AFM stage.
7. Focus the laser spot on the end of the cantilever and adjust the photodiode signal according to the AFM manufacturer's guidelines.
   ▲ CRITICAL STEP Make sure that the cantilever is fully immersed in the cell medium and there are no air bubbles trapped near the cantilever.
8. Set up the optical microscope. Select the appropriate objective, focus on the cells, and select the location for further AFM experiments.

Calibrations ● Timing 15 min

9. Calibrate the InvOLS (inverted optical lever sensitivity, in nanometers per Volt) by recording the thermal noise spectrum of the cantilever. To avoid surface-induced artifacts, the cantilever must be located at a distance of at least 100 μm from the bottom surface of the Petri dish. Use the relevant AFM software, which enables users to infer InvOLS through the analysis of thermal noise. A cantilever spring constant (k) must be provided for calibration.
   ▲ CRITICAL STEP It is highly recommended to use cantilevers for which the spring constant was precalibrated by an independent method (such as laser Doppler vibrometry). Alternatively, precalibration could be done by AFM from the analysis of thermal noise in air with the Sader method[93]. A recent study has shown that calibration of InvOLS from thermal noises in liquid is more reliable than calibration from the force curves obtained on a hard surface[94].
10. Select the iDrive mode and tune the cantilever. Tuning the iDrive cantilever in liquid is similar to tuning the piezo-driven cantilever in air; follow the guidelines of the AFM manufacturer. After a position of the peak is found, adjust the oscillation amplitude to 10–20 nm (this is the amplitude far from the sample). The phase signal should be adjusted to a specific value based

on the cantilever quality factor (Supplementary Theory), or a correction value could be introduced later during the data processing. The deflection signal should be zeroed. For multi-frequency mapping, the second eigenmode should be tuned in this step too. Adjust the oscillation amplitude of the second eigenmode to ~3–6 nm, and adjust the phase signal the same way as for the first eigenmode.

▲ **CRITICAL STEP** The values of drive frequency (ω_{dr}), quality factor (Q), amplitude (A_{1far}), and phase (ϕ_{1far} (A_{2far} and ϕ_{2far} if used)) should be recorded for further data processing.

▲ **CRITICAL STEP** For the iDrive mode, the driving voltage should not be higher than 1–2 V, as higher voltages might lead to increased electrochemistry reactions on the cantilever surface and its deterioration. In addition, high voltages may damage live cells.

? TROUBLESHOOTING

AFM imaging (mechanics experiment) ● Timing 15 min per cell

11. Perform the approach with the cantilever onto a blank place on the glass surface adjacent to the cells of interest. The approach can be done in contact mode.

    ▲ **CRITICAL STEP** The cantilever should not be too close to the surface of the dish, in order to have enough z-piezo range for the scanning. It is better to approach the clean surface near the cell than to approach the cell directly to avoid possible cell damage.

12. Place the cantilever above the cell of interest, near its central region (usually over the nucleus), and record a force curve with deflection, amplitude, and phase. From this curve, determine the values of A_{1near} and ϕ_{1near} as described in the Introduction (Fig. 2).

13. Select the scan size (ranging from 50 × 50 μm to 90 × 90 μm) to observe the entire or a large part of the cell, and the number of points (256 × 256 or 512 × 512), depending on the required resolution. First, a low-resolution scan can be obtained for adjustment of the scanning parameters.

14. Select the following channels for recording during the scanning: z-sensor signal (height), deflection (A_0), amplitude (A_1), and phase (φ_1 (A_{2far} and $\phi_{2far}$for multi-frequency mapping)).

15. Switch the feedback from conventional resonant frequency oscillation amplitude (A_1) to cantilever mean deflection (A_0). This will allow the use of higher scanning speeds.

16. Start with slow scanning speeds (from 0.25 to 0.5 Hz) and adjust the scanning parameters (set-point and feedback gain) for the best result. When feedback is applied to cantilever mean deflection, adjustment of the parameters is similar to such adjustment in the contact mode. Use the lowest deflection set-point (usually <0.5–1 nN) providing a stable tip–surface contact. Increase the feedback gain until the feedback oscillation can be seen in the deflection signal, and then decrease it slightly below the oscillation level. The scanning speed can be increased further (up to 6 Hz) if the quality of the images does not deteriorate substantially. Generally, smaller scan sizes allow the use of higher scanning speeds.

    ▲ **CRITICAL STEP** If instability is observed, reduce the scan rate until the instability disappears. On the optical microscope image, check that the cell is still attached and undamaged.

    ? TROUBLESHOOTING

17. At the end of the experiment, clean the cantilever and the cantilever holder. Because the cantilever and cantilever holder are in contact with the cell medium, they tend to become contaminated with proteins and lipids derived from the cell membrane. It is highly recommended to clean the cantilever and holder in the cleaning solution and then in ultrapure water to prevent salt crystallization.

Processing of the AFM data ● Timing 15 min per image

18. Import the acquired maps into MATLAB and run the script for data processing (available as the Supplementary Data). Input the experimental parameters: k_{cant}, ω_{dr}, Q_{far},A_{1far}, ϕ_{1far}, A_{1near}, and ϕ_{1near}.

19. Select the appropriate mechanical model. For living cells, the optimal model is the Sneddon model with bottom-effect correction. The output will contain the maps of interaction forces ($F^n_{ts,CONS}$ and $F^n_{ts,DISS}$) and sample mechanical parameters ($k^{dynamic}_{sample}$, $c^{dynamic}_{sample}$, $E^{storage}_{BECC}$, and E^{loss}_{BECC}).

Troubleshooting

Troubleshooting advice can be found in Table 1.

Table 1 | Troubleshooting table

Step	Problem	Possible reason	Solution
10	No peak appears while tuning the cantilever	The cantilever or its coating is damaged	Check that the laser alignment was done properly. Try another cantilever
16	Many strokes on the AFM image, overall low quality of the image	The cell is weakly attached to the surface or was damaged by the cantilever	Check that the cell is well attached and looks healthy under the optical microscope. If you can see movement of the cell parts caused by the cantilever during the scanning, select another cell for imaging and use a lower force set-point. If the problems recur, try modifying the experimental conditions (surface coating, pH, temperature, and cell density)
	Unstable AFM signals while not scanning	Dead cell/debris attached to the cantilever	Lift the AFM head high enough to remove the cantilever from the liquid completely. The cell should be detached by the surface tension of the air–water interface. Repeat a few times. If this does not help, wash the cantilever in the detergent solution, or replace it with a new one

Timing

Steps 1 and 2, preparation of cells for AFM: 15 min, followed by 1–2 d of culture
Steps 3–8, setup of the AFM and optical microscope: 15 min
Steps 9 and 10, calibrations: 15 min
Steps 11–17, AFM imaging (mechanics experiment): 15 min per cell
Steps 18 and 19, processing of the AFM data: 15 min per image

Anticipated results

Maps of cell mechanical properties to study normal and pathophysiology of cells

In addition to the topographical data, the current protocol will enable users to obtain maps of the mean deflection, and amplitude and phase maps for each excitation frequency used as observables. Following the data analysis described in Steps 18 and 19 will provide the corresponding $k_{\text{sample}}^{\text{dynamic}}$ and $c_{\text{sample}}^{\text{dynamic}}$ maps. If applicable, such as in the case of soft living cells, it will also calculate the local elastic complex modulus and mean indentation depth at each point for the selected mechanical contact model. The preferable model for thin samples such as cells would be the BECC model, but the Sneddon model could be used for thicker regions and low indentation depths. Fine details of sub-surface features such as actin filament bundles (stress fibers) and the nuclear complex are clearly displayed in the physical property maps of fibroblasts (Fig. 1). Optionally, these maps can be compared with the fluorescence images of the cytoskeleton or any other cellular structure.

We have demonstrated the large intracellular heterogeneity in local mechanical properties of different living cells with the approach described in this protocol[28,37,43,95]. For adherent fibroblasts, the stress fibers are visible on the nanomechanical maps as stiffer structures that can be confirmed with fluorescence images (Fig. 1 and Fig. 3). In the growth cone of the *Aplysia* bag cell neuron, different domains can be distinguished by mapping the mechanical properties[96]. In the peripheral domain, the presence of filopodial actin bundles correlates to stiffer regions as compared with intermittent lamellipodial actin networks (Fig. 4, Supplementary Fig. 1). The central domain is stiffer, which is consistent with the fact that it is filled with tightly packed microtubules.

The high temporal resolution of this method (only 10 s of image acquisition time per frame on standard commercial AFM systems) enables the study of dynamic changes in cellular properties. For example, we investigated the mechanical response of MDA-MB-231 breast carcinoma cells to the inhibition of spleen tyrosine kinase (Syk) proteins with high spatiotemporal resolution, providing insight into the signaling pathways by which Syk negatively regulates the motility of highly invasive cancer cells[28]. In the E^{storage}maps (Fig. 5) and the AFM multi-harmonic observable maps (Supplementary Fig. 2), rapid changes in the cell periphery were observed that included a retraction of the leading edge with a marked increase in F-actin retrograde flow and disassembly of focal adhesions after addition of the Syk-AQL-EGFP inhibitor. These marked re-arrangements in the actin

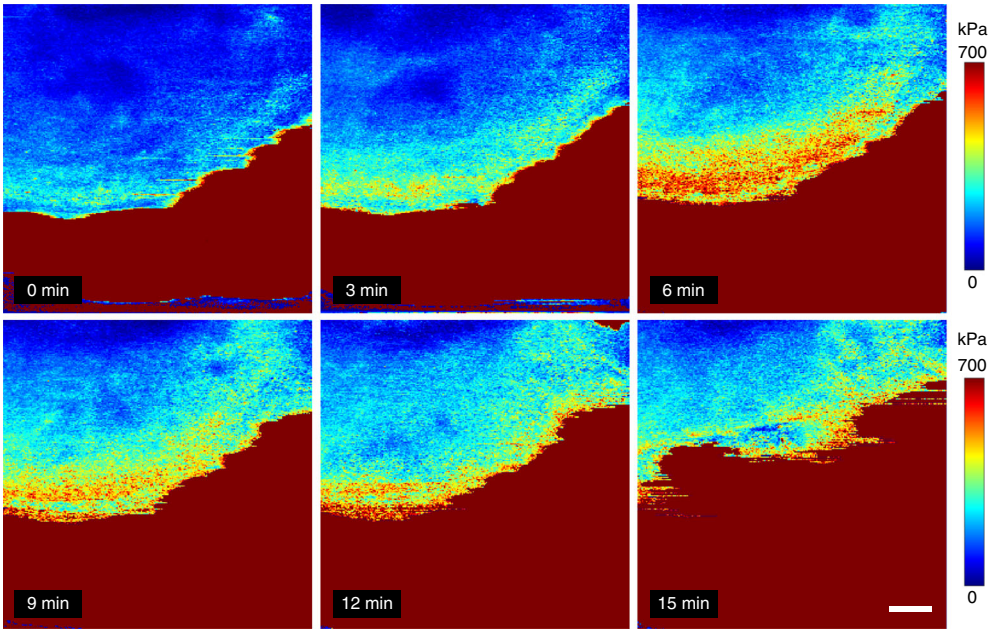

Fig. 5 | Tracking the fast temporal changes in nanomechanical heterogeneities of MDA-MB-231 breast cancer cells upon inhibition of Syk-AQL-EGFP protein tyrosine kinase with 1-NM-PP1. The rapid loss of Syk activity was correlated with marked rearrangements in the cortical actin cytoskeleton, observed as a retraction of the leading edge[28]. Only the storage elastic modulus ($E^{storage}$) is shown here. The acquisition time was 1 min 30 s (256 × 256 pixels); every second image in the series is shown. Scale bar, 5 μm.

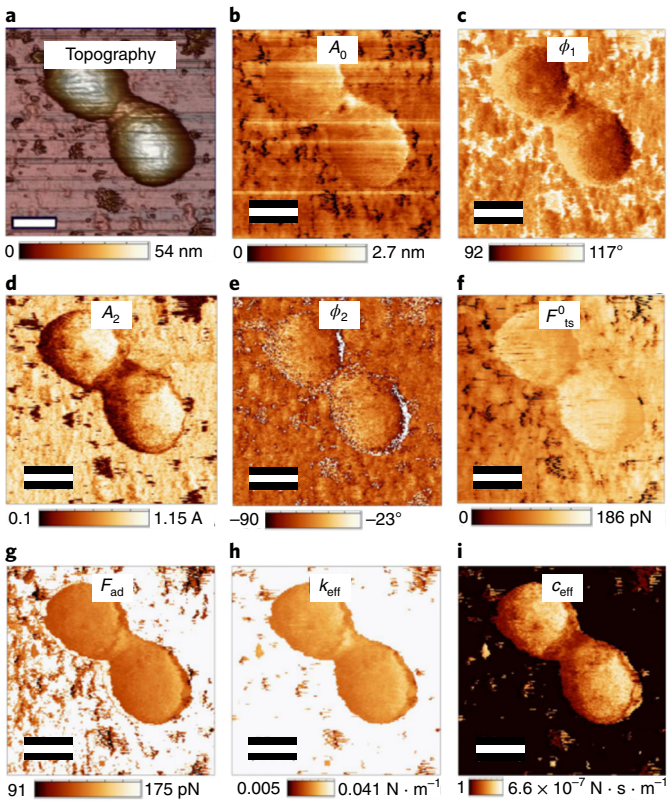

Fig. 6 | Property maps of ϕ29 bacteriophage mature virions. a, 3D-rendered topography image of bacteriophage ϕ29 using a Lorentz excited cantilever showing two well-defined virions. **b**–**e**, Multi-harmonic data (A_0 (**b**), ϕ_1 (**c**), A_2 (**d**), and ϕ_2 (**e**)) recorded simultaneously with topography. **f**, The applied force map F^0_{ts} value at which the imaging was done during the experiment. **g**–**i**, Maps of the local material properties: adhesion force (pN, **g**), local effective stiffness (N · m^{-1}, **h**), and effective viscosity (N · s · m^{-1}, **i**). Scale bars, 55 nm. Adapted with –permission from Cartagena et al.[44], Royal Society of Chemistry.

cytoskeleton are consistent with reports of Syk modulating cortical actin dynamics in B cells and platelets[97,98]. Temporal resolution can be further improved in the next-generation high-speed AFMs, particularly because the approach described in this protocol is perfectly compatible with such systems.

The spatial resolution of the method depends on the selected cantilevers (see Experimental design) and the mechanical properties of the sample, because of the effects of both these parameters on the tip–sample contact area during the scanning[99]. For living cells, the contact area will be larger than that for the stiff virion shells or bacteria cell walls, and the resolution will be lower. However, the individual stress fibers or actin bundles can still be resolved, meaning that the spatial resolution is on the order of tens to hundreds of nanometers. For relatively stiff samples such as viruses, the electromechanical force gradient, adhesion, and hydration layer viscosity can be mapped within individual ϕ29 bacteriophage mature virions (Fig. 6). The spatial resolution of the method allowed study of the local disruption of the virion shell[44] with resolution on the order of several nanometers.

In summary, we believe that the described protocol and computational algorithms are sufficient for AFM users to move from standard AFM imaging to more advanced quantitative nanomechanical mapping.

Reporting Summary

Further information on experimental design is available in the Nature Research Reporting Summary linked to this article.

References

1. Nelson, C. M. et al. Emergent patterns of growth controlled by multicellular form and mechanics. *Proc. Natl. Acad. Sci. USA* **102**, 11594–11599 (2005).
2. Wang, N., Tytell, J. D. & Ingber, D. E. Mechanotransduction at a distance: mechanically coupling the extracellular matrix with the nucleus. *Nat. Rev. Mol. Cell Biol.* **10**, 75–82 (2009).
3. Rotsch, C., Jacobson, K. & Radmacher, M. Dimensional and mechanical dynamics of active and stable edges in motile fibroblasts investigated by using atomic force microscopy. *Proc. Natl. Acad. Sci. USA* **96**, 921–926 (1999).
4. Lange, J. R. & Fabry, B. Cell and tissue mechanics in cell migration. *Exp. Cell Res.* **319**, 2418–2423 (2013).
5. Friedl, P., Wolf, K. & Lammerding, J. Nuclear mechanics during cell migration. *Curr. Opin. Cell Biol.* **23**, 55–64 (2011).
6. Franze, K., Janmey, P. A. & Guck, J. Mechanics in neuronal development and repair. *Annu. Rev. Biomed. Eng.* **15**, 227–251 (2013).
7. Kumar, S. & Weaver, V. M. Mechanics, malignancy, and metastasis: the force journey of a tumor cell. *Cancer Metastasis Rev.* **28**, 113–127 (2009).
8. Wirtz, D., Konstantopoulos, K. & Searson, P. C. The physics of cancer: the role of physical interactions and mechanical forces in metastasis. *Nat. Rev. Cancer* **11**, 512–522 (2011).
9. Suresh, S. Biomechanics and biophysics of cancer cells. *Acta Mater.* **55**, 3989–4014 (2007).
10. Rotsch, C. & Radmacher, M. Drug-induced changes of cytoskeletal structure and mechanics in fibroblasts: an atomic force microscopy study. *Biophys. J.* **78**, 520–535 (2000).
11. Efremov, Y. M. et al. Distinct impact of targeted actin cytoskeleton reorganization on mechanical properties of normal and malignant cells. *Biochim. Biophys. Acta* **1853**, 3117–3125 (2015).
12. Grady, M. E., Composto, R. J. & Eckmann, D. M. in *Mechanics of Biological Systems and Materials* (eds. Barthelat, F., Zavattieri, P., Korach, C. S., Prorok, B. C. & Grande-Allen, K. J.) **6**, 169–177 (Springer, New York, 2017).
13. Cross, S. E., Jin, Y. S., Rao, J. & Gimzewski, J. K. Nanomechanical analysis of cells from cancer patients. *Nat. Nanotechnol.* **2**, 780–783 (2007).
14. Lekka, M. et al. Cancer cell recognition–mechanical phenotype. *Micron* **43**, 1259–1266 (2012).
15. van Zwieten, R. W. et al. Assessing dystrophies and other muscle diseases at the nanometer scale by atomic force microscopy. *Nanomedicine* **9**, 393–406 (2014).
16. Burridge, K. & Guilluy, C. Focal adhesions, stress fibers and mechanical tension. *Exp. Cell Res.* **343**, 14–20 (2016).
17. Ingber, D. E., Wang, N. & Stamenovic, D. Tensegrity, cellular biophysics, and the mechanics of living systems. *Rep. Prog. Phys.* **77**, 046603 (2014).
18. Plotnikov, S. V., Pasapera, A. M., Sabass, B. & Waterman, C. M. Force fluctuations within focal adhesions mediate ECM-rigidity sensing to guide directed cell migration. *Cell* **151**, 1513–1527 (2012).
19. Park, C. Y. et al. Mapping the cytoskeletal prestress. *Am. J. Physiol. Cell Physiol.* **298**, C1245–C1252 (2010).
20. Hochmuth, R. M. Micropipette aspiration of living cells. *J. Biomech.* **33**, 15–22 (2000).
21. Desprat, N., Richert, A., Simeon, J. & Asnacios, A. Creep function of a single living cell. *Biophys. J.* **88**, 2224–2233 (2005).

22. Caille, N., Thoumine, O., Tardy, Y. & Meister, J. J. Contribution of the nucleus to the mechanical properties of endothelial cells. *J. Biomech.* **35**, 177–187 (2002).
23. Ayala, Y. A. et al. Rheological properties of cells measured by optical tweezers. *BMC Biophys.* **9**, 5 (2016).
24. Wei, M.-T. et al. A comparative study of living cell micromechanical properties by oscillatory optical tweezers. *Opt. Express* **16**, 8594–8603 (2008).
25. Hu, S. et al. Mechanical anisotropy of adherent cells probed by a three-dimensional magnetic twisting device. *Am. J. Physiol. Cell Physiol.* **287**, C1184–C1191 (2004).
26. Hoffman, B. D., Massiera, G., Van Citters, K. M. & Crocker, J. C. The consensus mechanics of cultured mammalian cells. *Proc. Natl. Acad. Sci. USA* **103**, 10259–10264 (2006).
27. Haga, H. et al. Elasticity mapping of living fibroblasts by AFM and immunofluorescence observation of the cytoskeleton. *Ultramicroscopy* **82**, 253–258 (2000).
28. Cartagena-Rivera, A. X., Wang, W.-H., Geahlen, R. L. & Raman, A. Fast, multi-frequency, and quantitative nanomechanical mapping of live cells using the atomic force microscope. *Sci. Rep.* **5**, 11692 (2015).
29. A-Hassan, E. et al. Relative microelastic mapping of living cells by atomic force microscopy. *Biophys. J.* **74**, 1564–1578 (1998).
30. Kuznetsova, T. G., Starodubtseva, M. N., Yegorenkov, N. I., Chizhik, S. A. & Zhdanov, R. I. Atomic force microscopy probing of cell elasticity. *Micron* **38**, 824–833 (2007).
31. Gavara, N. A beginner's guide to atomic force microscopy probing for cell mechanics. *Microsc. Res. Tech.* 1–10 (2016).
32. Efremov, Y. M., Wang, W.-H., Hardy, S. D., Geahlen, R. L. & Raman, A. Measuring nanoscale viscoelastic parameters of cells directly from AFM force-displacement curves. *Sci. Rep.* **7**, 1541 (2017).
33. Rico, F. et al. Probing mechanical properties of living cells by atomic force microscopy with blunted pyramidal cantilever tips. *Phys. Rev. E* **72**, 21914 (2005).
34. Radmacher, M. Measuring the elastic properties of living cells by the atomic force microscope. *Methods Cell Biol.* **68**, 67–90 (2002).
35. Garcia, P. D., Guerrero, C. R. & Garcia, R. Time-resolved nanomechanics of a single cell under the depolymerization of the cytoskeleton. *Nanoscale* **9**, 12051–12059 (2017).
36. Brückner, B. R., Nöding, H. & Janshoff, A. Viscoelastic properties of confluent MDCK II cells obtained from force cycle experiments. *Biophys. J.* **112**, 724–735 (2017).
37. Raman, A. et al. Mapping nanomechanical properties of live cells using multi-harmonic atomic force microscopy. *Nat. Nanotechnol.* **6**, 809–814 (2011).
38. Sahin, O. et al. High-resolution imaging of elastic properties using harmonic cantilevers. *Sens. Actuators A Phys.* **114**, 183–190 (2004).
39. van Noort, S. J. T., Willemsen, O. H., van der Werf, K. O., de Grooth, B. G. & Greve, J. Mapping electrostatic forces using higher harmonics tapping mode atomic force microscopy in liquid. *Langmuir* **15**, 7101–7107 (1999).
40. Dufrêne, Y. F. et al. Imaging modes of atomic force microscopy for application in molecular and cell biology. *Nat. Nanotechnol.* **12**, 295–307 (2017).
41. Chyasnavichyus, M., Young, S. L. & Tsukruk, V. V. Recent advances in micromechanical characterization of polymer, biomaterial, and cell surfaces with atomic force microscopy. *Jpn. J. Appl. Phys.* **54**, 08LA02 (2015).
42. Tung, R. C., Jana, A. & Raman, A. Hydrodynamic loading of microcantilevers oscillating near rigid walls. *J. Appl. Phys.* **104**, 114905 (2008).
43. Cartagena, A. & Raman, A. Local viscoelastic properties of live cells investigated using dynamic and quasi-static atomic force microscopy methods. *Biophys. J.* **106**, 1033–1043 (2014).
44. Cartagena, A., Hernando-Pérez, M., Carrascosa, J. L., de Pablo, P. J. & Raman, A. Mapping in vitro local material properties of intact and disrupted virions at high resolution using multi-harmonic atomic force microscopy. *Nanoscale* **5**, 4729–4736 (2013).
45. Melcher, J. et al. Origins of phase contrast in the atomic force microscope in liquids. *Proc. Natl. Acad. Sci. USA* **106**, 13655–13660 (2009).
46. Xu, X., Melcher, J., Basak, S., Reifenberger, R. & Raman, A. Compositional contrast of biological materials in liquids using the momentary excitation of higher eigenmodes in dynamic atomic force microscopy. *Phys. Rev. Lett.* **102**, 060801 (2009).
47. Hertz, H. Über die Berührung Fester Elastischer Körper. *J. reine u. angew. Math.* **92**, 156–171 (1881).
48. Sneddon, I. N. The relation between load and penetration in the axisymmetric Boussinesq problem for a punch of arbitrary profile. *Int. J. Eng. Sci.* **3**, 47–57 (1965).
49. Dimitriadis, E. K., Horkay, F., Maresca, J., Kachar, B. & Chadwick, R. S. Determination of elastic moduli of thin layers of soft material using the atomic force microscope. *Biophys. J.* **82**, 2798–2810 (2002).
50. Gavara, N. & Chadwick, R. S. Determination of the elastic moduli of thin samples and adherent cells using conical atomic force microscope tips. *Nat. Nanotechnol.* **7**, 733–736 (2012).
51. Krisenko, M. O., Cartagena, A., Raman, A. & Geahlen, R. L. Nanomechanical property maps of breast cancer cells as determined by multiharmonic atomic force microscopy reveal Syk-dependent changes in microtubule stability mediated by MAP1B. *Biochemistry* **54**, 60–68 (2015).
52. Kronlage, C., Schäfer-Herte, M., Böning, D., Oberleithner, H. & Fels, J. Feeling for filaments: quantification of the cortical actin web in live vascular endothelium. *Biophys. J.* **109**, 687–698 (2015).

53. Smolyakov, G., Formosa-Dague, C., Severac, C., Duval, R. E. & Dague, E. High speed indentation measures by FV, QI and QNM introduce a new understanding of bionanomechanical experiments. *Micron* **85**, 8–14 (2016).
54. Schillers, H., Medalsy, I., Hu, S., Slade, A. L. & Shaw, J. E. PeakForce tapping resolves individual microvilli on living cells. *J. Mol. Recognit.* **29**, 95–101 (2016).
55. Calzado-Martín, A., Encinar, M., Tamayo, J., Calleja, M. & San Paulo, A. Effect of actin organization on the stiffness of living breast cancer cells revealed by peak-force modulation atomic force microscopy. *ACS Nano* (2016). https://doi.org/10.1021/acsnano.5b07162.
56. Ando, T. Directly watching biomolecules in action by high-speed atomic force microscopy. *Biophys. Rev.* **9**, 421–429 (2017).
57. Vogel, V. & Sheetz, M. P. Cell fate regulation by coupling mechanical cycles to biochemical signaling pathways. *Curr. Opin. Cell Biol.* **21**, 38–46 (2009).
58. Xu, X. & Raman, A. Comparative dynamics of magnetically, acoustically, and Brownian motion driven microcantilevers in liquids. *J. Appl. Phys.* **102**, 034303 (2007).
59. Enders, O., Korte, F. & Kolb, H.-A. Lorentz-force-induced excitation of cantilevers for oscillation-mode scanning probe microscopy. *Surf. Interface Anal.* **36**, 119–123 (2004).
60. Kiracofe, D., Kobayashi, K., Labuda, A., Raman, A. & Yamada, H. High efficiency laser photothermal excitation of microcantilever vibrations in air and liquids. *Rev. Sci. Instrum.* **82**, 013702 (2011).
61. Labuda, A. et al. Comparison of photothermal and piezoacoustic excitation methods for frequency and phase modulation atomic force microscopy in liquid environments. *AIP Adv.* **1**, 022136 (2011).
62. Rabe, U. & Arnold, W. Acoustic microscopy by atomic force microscopy. *Appl. Phys. Lett.* **64**, 1493–1495 (1994).
63. Schäffer, T. E., Cleveland, J. P., Ohnesorge, F., Walters, D. A. & Hansma, P. K. Studies of vibrating atomic force microscope cantilevers in liquid. *J. Applied Physics* **80**, 3622 (2012).
64. Kiracofe, D. & Raman, A. Quantitative force and dissipation measurements in liquids using piezo-excited atomic force microscopy: a unifying theory. *Nanotechnology* **22**, 485502 (2011).
65. Florin, E.-L., Radmacher, M., Fleck, B. & Gaub, H. E. Atomic force microscope with magnetic force modulation. *Rev. Sci. Instrum.* **65**, 639 (1994).
66. Han, W., Lindsay, S. M. & Jing, T. A magnetically driven oscillating probe microscope for operation in liquids. *Appl. Phys. Lett.* **69**, 4111–4113 (1996).
67. Ge, G. et al. MAC mode atomic force microscopy studies of living samples, ranging from cells to fresh tissue. *Ultramicroscopy* **107**, 299–307 (2007).
68. Wang, A., Butte, M. J., Wang, A. & Butte, M. J. Customized atomic force microscopy probe by focused-ion-beam-assisted tip transfer. *Appl. Phys. Lett.* **105**, 053101 (2015).
69. Nagao, E. & Dvorak, J. A. An integrated approach to the study of living cells by atomic force microscopy. *J. Microsc.* **191**, 8–19 (1998).
70. Garcia, R. & Herruzo, E. T. The emergence of multifrequency force microscopy. *Nat. Nanotechnol.* **7**, 217–226 (2012).
71. Garcia, R. & Proksch, R. Nanomechanical mapping of soft matter by bimodal force microscopy. *Eur. Polym. J.* **49**, 1897–1906 (2013).
72. Solares, S. D. & Chawla, G. Frequency response of higher cantilever eigenmodes in bimodal and trimodal tapping mode atomic force microscopy. *Meas. Sci. Technol.* **21**, 125502 (2010).
73. Balland, M. et al. Power laws in microrheology experiments on living cells: comparative analysis and modeling. *Phys. Rev. E* **74**, 021911 (2006).
74. Alcaraz, J. et al. Microrheology of human lung epithelial cells measured by atomic force microscopy. *Biophys. J.* **84**, 2071–2079 (2003).
75. Rigato, A., Miyagi, A., Scheuring, S. & Rico, F. High-frequency microrheology reveals cytoskeleton dynamics in living cells. *Nat. Phys.* (2017). https://doi.org/10.1038/nphys4104.
76. Kollmannsberger, P. & Fabry, B. Linear and nonlinear rheology of living cells. *Annu. Rev. Mater. Res.* **41**, 75–97 (2011).
77. Jonas, O. & Duschl, C. Force propagation and force generation in cells. *Cytoskeleton* **67**, 555–563 (2010).
78. Silberberg, Y. R. et al. Mitochondrial displacements in response to nanomechanical forces. *J. Mol. Recognit.* **21**, 30–36 (2008).
79. Krause, M., te Riet, J. & Wolf, K. Probing the compressibility of tumor cell nuclei by combined atomic force–confocal microscopy. *Phys. Biol.* **10**, 065002 (2013).
80. Rosenbluth, M. J., Crow, A., Shaevitz, J. W. & Fletcher, D. A. Slow stress propagation in adherent cells. *Biophys. J.* **95**, 6052–6059 (2008).
81. Lim, S.-M., Trzeciakowski, J. P., Sreenivasappa, H., Dangott, L. J. & Trache, A. RhoA-induced cytoskeletal tension controls adaptive cellular remodeling to mechanical signaling. *Integr. Biol.* **4**, 615 (2012).
82. Melzak, Ka & Toca-Herrera, J. L. Atomic force microscopy and cells: indentation profiles around the AFM tip, cell shape changes, and other examples of experimental factors affecting modeling. *Microsc. Res. Tech.* **78**, 626–632 (2015).
83. Trache, A. & Lim, S.-M. Integrated microscopy for real-time imaging of mechanotransduction studies in live cells. *J. Biomed. Opt.* **14**, 034024 (2009).

84. Staunton, J. R., Doss, B. L., Lindsay, S. & Ros, R. Correlating confocal microscopy and atomic force indentation reveals metastatic cancer cells stiffen during invasion into collagen I matrices. *Sci. Rep.* **6**, 19686 (2016).
85. Cascione, M., de Matteis, V., Rinaldi, R. & Leporatti, S. Atomic force microscopy combined with optical microscopy for cells investigation. *Microsc. Res. Tech.* **80**, 109–123 (2017).
86. Charras, G. T. & Horton, M. A. Determination of cellular strains by combined atomic force microscopy and finite element modeling. *Biophys. J.* **83**, 858–879 (2002).
87. Jonkman, J. & Brown, C. M. Any way you slice it-a comparison of confocal microscopy techniques. *J. Biomol. Tech.* **26**, 54–65 (2015).
88. Lulevich, V., Shih, Y. P., Lo, S. H. & Liu, G. Cell tracing dyes significantly change single cell mechanics. *J. Phys. Chem. B* **113**, 6511–6519 (2009).
89. Sliogeryte, K. et al. Differential effects of LifeAct-GFP and actin-GFP on cell mechanics assessed using micropipette aspiration. *J. Biomech.* **49**, 310–317 (2016).
90. Lee, A. C., Decourt, B. & Suter, D. Neuronal cell cultures from *Aplysia* for high-resolution imaging of growth cones. *J. Vis. Exp*. (2008). https://doi.org/10.3791/662.
91. Suter, D. M. in *Cell Migration. Methods in Molecular Biology (Methods and Protocols)* (eds. Wells, C. & Parsons, M.) 65–86 (Humana Press, New York, 2011).
92. Lukinavičius, G. et al. Fluorogenic probes for live-cell imaging of the cytoskeleton. *Nat. Methods* **11**, 731–3 (2014).
93. Sader, J. E. et al. A virtual instrument to standardise the calibration of atomic force microscope cantilevers. *Rev. Sci. Instrum*. **87**, 093711 (2016).
94. Schillers, H. et al. Standardized nanomechanical atomic force microscopy procedure (SNAP) for measuring soft and biological samples. *Sci. Rep.* **7**, 5117 (2017).
95. Hernando-Pérez, M. et al. Quantitative nanoscale electrostatics of viruses. *Nanoscale* **7**, 17289–17298 (2015).
96. Xiong, Y., Lee, A. C., Suter, D. M. & Lee, G. U. Topography and nanomechanics of live neuronal growth cones analyzed by atomic force microscopy. *Biophys. J.* **96**, 5060–5072 (2009).
97. Gallet, C. et al. Tyrosine phosphorylation of cortactin associated with Syk accompanies thromboxane analogue-induced platelet shape change. *J. Biol. Chem.* **274**, 23610–23616 (1999).
98. Le Roux, D. et al. Syk-dependent actin dynamics regulate endocytic trafficking and processing of antigens internalized through the B-cell receptor. *Mol. Biol. Cell* **18**, 3451–3462 (2007).
99. Braet, F., Rotsch, C., Wisse, E. & Radmacher, M. Comparison of fixed and living liver endothelial cells by atomic force microscopy. *Appl. Phys. A Mater. Sci. Process.* **66**, 575–578 (1998).

Acknowledgements

This work was supported by the Incentive Grant Program of the Office of the Executive Vice President for Research and Partnerships – Purdue University (D.M.S. and A.R.) and by NSF 1146944-IOS (D.M.S.). A.X.C.-R. was supported by intramural funding from the Division of Intramural Research Program at the National Institute on Deafness and Other Communication Disorders.

Author contributions

A.X.C.-R., Y.M.E., D.M.S., and A.R. conceived and designed the experiments. Y.M.E., A.X.C.-R., A.I.M.A., D.M.S., and A.R. developed experimental protocols for sample preparation. Y.M.E. and A.X.C.-R. performed all the research experiments, analyzed the data, and prepared the figures. Y.M.E., A.X.C.-R., D.M.S., and A.R. co-wrote the paper. All authors discussed the results and reviewed the paper.

Competing interests

The authors declare no competing interests.

Additional information

Supplementary information is available for this paper at https://doi.org/10.1038/s41596-018-0031-8.

Reprints and permissions information is available at www.nature.com/reprints.

Correspondence and requests for materials should be addressed to A.R.

Publisher's note: Springer Nature remains neutral with regard to jurisdictional claims in published maps and institutional affiliations.

Published online: 14 September 2018

Related links

Key references using this protocol

Raman, A. et al. *Nat. Nanotechnol.* **6**, 809–814 (2011) https://doi.org/10.1038/nnano.2011.186

Cartagena, A., Hernando-Pérez, M., Carrascosa, J. L., de Pablo, P. J. & Raman, A. *Nanoscale* **5**, 4729–4736 (2013) https://doi.org/10.1039/C3NR34088K

Cartagena-Rivera, A. X., Wang, W.-H., Geahlen, R. L. & Raman, A. *Sci. Rep.* **5**, 11692 (2015) https://doi.org/10.1038/srep11692